Electron Beam Lithography and Evaporation on Ultra-thin Silicon Nitride Membranes

- Target Manufacturing for Digital Holography

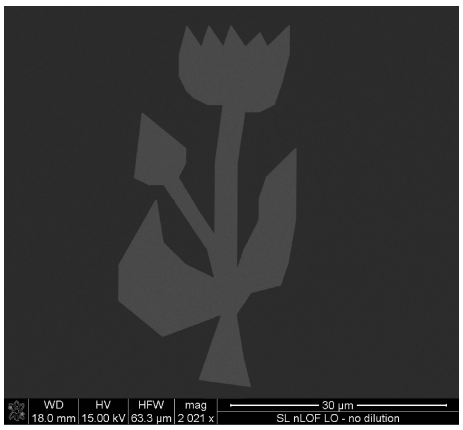

Diploma Thesis, 30 ECTS,
by
Eleonora Lorek

Lund Reports on Atomic Physics, LRAP-416
Lund, April 2010

LUNDS UNIVERSITET

Abstract

Microscopy is fascinating and gives access to part of the world not directly available to us. There are many well-developed microscopy techniques and things as small as atoms can be seen. However, *time-resolved* microscopy is something new. Studying processes with a very high time resolution would also give us access to a new part of the world, previously unseen. This thesis explores the possibilities of the digital holography setup in Lund, based on a powerful terawatt laser system, that has a potential to become a time-resolved microscope. The properties investigated are its spatial resolution and its capability to reconstruct phase of light. These capabilities are explored by manufacturing and applying suitable targets, targets made by electron beam lithography and evaporation on 20 nm thin silicon nitride membranes in the Lund Nano Lab.

Contents

1 Introduction **1**
- 1.1 Background . . . 1
- 1.2 Aim of Report . . . 2
- 1.3 Outline of Report . . . 2

2 Theoretical Considerations **3**
- 2.1 Digital In-line Holography . . . 3
- 2.2 Resolution of Space and Reconstruction of Phase . . . 6
- 2.3 Targets . . . 7
  - 2.3.1 Choice of Target Design . . . 7
  - 2.3.2 Choice of Processing Method . . . 8
  - 2.3.3 Choice of Characterization Method . . . 16

3 Target Processing **18**
- 3.1 Preparation . . . 18
- 3.2 Spin Coating . . . 19
- 3.3 Exposure . . . 21
- 3.4 Development . . . 26
- 3.5 Evaporation . . . 26
- 3.6 Lift-off . . . 28

4 Target Characterization **29**

5 Holography **31**
- 5.1 Experimental Method . . . 31
- 5.2 Results . . . 32

6 Discussion and Outlook **35**

1 Introduction

1.1 Background

This diploma thesis is part of a project with the final goal to do time resolved microscopy. This means obtaining clear images of rapid processes in small objects.

One way to achieve this goal is to use a coherent light source producing light of short wavelength and short pulse duration. These features enable a high spatial and temporal resolution. The light source illuminates the object whereupon light is scattered into a diffraction pattern. The pattern can be used to reconstruct the electric field in the plane of the object by Fourier transformation. The recorded intensity at a certain position in the detector plane corresponds to a wave with a certain amplitude and frequency in the object plane. These waves constitute the electric field in the object plane. The reconstruction of the electric field function requires not only the amplitude and frequency of the waves, but also the phase of the scattered waves in the detector plane. The loss of information about phase when making a measurement is known as the "phase problem" [3]. The phase must be known in order for the waves constituting the electric field function to have the correct relative position.

A prominent light source producing coherent light of short wavelength and short pulse duration is the FLASH free electron laser in Hamburg, Germany. This source was successfully used for time resolved diffractive imaging [5]. High-order harmonics generated when an intense laser interacts with a gas target constitute another interesting source. Several groups are working with time-resolved coherent imaging using High Harmonic Generation (HHG) [1], [15], [18] and [16].

HHG is also the approach taken in the coherent imaging setup in Lund. In the setup, the original light source is a titanium sapphire laser system, which produces pulses of 40 fs duration at 800 nm. The pulses are focused into an argon gas cell, where the generation takes place: the infrared pulses distort the coulomb potential of the gas atoms, allow for tunneling of electrons through the potential barrier, and accelerate the electrons onto a trajectory that permits recombination with the gas atoms. During the recombination process, odd harmonics of the fundamental frequency are emitted. The coherence and the short pulse duration are inherited from the laser, but now the wavelength is shorter.

The generated spectrum ranges into the X-UV regime, which is at wavelengths between 121 and 12 nm. Light in this wavelength range is absorbed by air and has to propagate in vacuum. The spectrum can be filtered with multilayer coated mirrors to select certain wavelengths. Here, a small bandwidth around 38 nm is selected, constituting the light source for the imaging.

As mentioned above, information about the phase of the diffracted light in the detector plane is needed to reconstruct the electric field function in the object plane. The phase can be retrieved by applying iterative algorithms, which use *a priori* knowledge of the object as a constraint in each iteration [6]. A more direct way is to use digital in-line holography. Here, the phase of the diffracted light is recovered through its interference with a reference wave with known phase. Hence the full electric field, with amplitude and phase, at the object plane can be determined.

The goal of this diploma work is to determine the spatial resolution of the holography method used in Lund and investigate its capability to reconstruct phase. Among the procedures involved in this, I have worked mainly with processing and characterization of suitable targets. I have also participated in the application of the targets to the setup.

1.2 Aim of Report

The aim of the report is to describe the type of targets produced, the spatial resolution of the holography method and its capability to reconstruct phase.

1.3 Outline of Report

Some theoretical considerations are made in section 2. The section includes a description of digital holography, a definition of "spatial resolution" and reasonings about phase reconstruction. What type of targets that is suitable to build is discussed. Choices of design and processing and characterization methods are made. The processing is described in section 3 and the made targets presented in section 4. Section 5 describes the targets applied to the holography setup: the experiment and the results. Section 6 is devoted to a discussion and an outlook.

2 Theoretical Considerations

Three central concepts need clarification: "digital in-line holography", "spatial resolution" and "reconstruction of phase". The meaning of these concepts will have bearing on the design, processing method and characterization method of the targets.

2.1 Digital In-line Holography

When we hear about holography (from the Greek *holo*: whole, *graphos*: drawing, writing) we might think of fascinating three-dimensional reconstructions of objects. It is easy to get puzzled when we look at one. It looks as if there is an object there, but at the same time the object seems transparent and when we reach out to touch it, there is nothing there. Maybe the feeling of it being an object there results from the 3D characteristics of the image.

Holography was discovered in 1947 by Dennis Gabor. The idea behind it is to split a coherent beam into one beam illuminating the object and one beam ("reference wave") that illuminates a photographic plate. In addition to the amplitude of the electric field in the hologram plane, the phase can be measured, as it is encoded in the interference pattern observed.

In off-line holography the two beams are completely separated and recombined where they are detected. Figure 1 illustrates the off-line recording of a hologram and figure 2 shows the off-line reconstruction of the electric field [8].

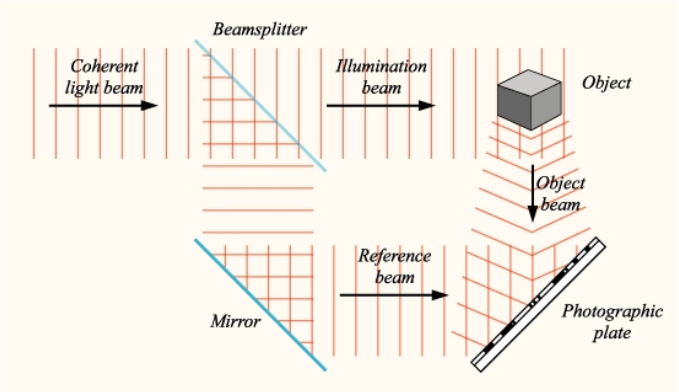

Figure 1: The recording of a hologram.

One can also record the interference pattern on a digital device like a CCD camera instead of a photographic plate. The reconstruction of the field is then done by an algorithm on a computer. This approach is called "digital holography". When the electric field is reconstructed, it is reconstructed in one plane, the object plane. The field contains information about how the amplitude and the phase of the field varies in the plane. The position of the plane should be thought of as just after the object. So if the amplitude is very low in one area, something just before the plane absorbed the light. For simplicity, reconstructions of *objects* will be discussed. This does really mean that we are reconstructing the field with amplitude and phase at the object plane.

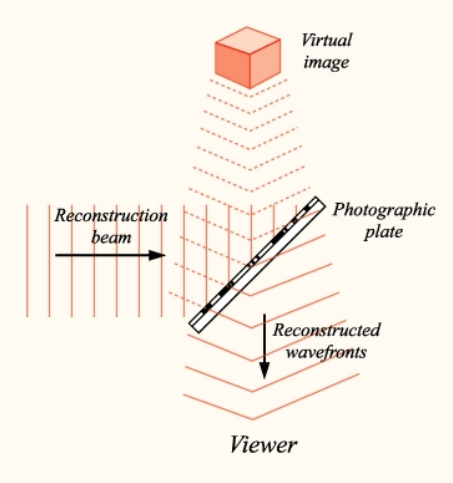

Figure 2: The reconstruction of the field.

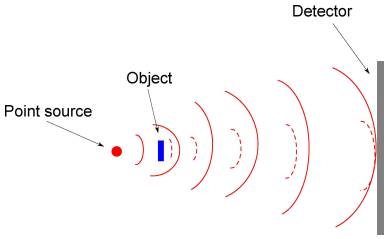

Figure 3: In-line holography.

In in-line holography the interference pattern consists of parts of a beam scattered by the object and parts of the same beam unaffected, see figure 3. Digital in-line holography is the approach taken in the present experiment. If one wants to use short wavelengths, this procedure is preferred to off-line holography. The reason is that at short wavelengths too much intensity would be lost at beam splitters and mirrors [13]- components used in the off-line setup. Another advantage with in-line holography is that stability is gained. There are not, as in the case with off-line holography, two beams that need to be perfectly recombined. Also, one has magnification due to the divergence.

The reconstruction algorithm is a process based on the Huygens-Fresnel principle [19], describing diffraction:

Every point of a wave front can be considered as a source point for secondary spherical waves. The wavefront at any other place is the coherent superposition of these secondary waves.

The Fresnel-Kirchhoff diffraction integral expresses this principle mathematically [19]. It can be written as follows [13]:

$$E_H(x_H, y_H) = \frac{i}{\lambda} \int_{-\infty}^{+\infty} \int_{-\infty}^{+\infty} E_O(x_O, y_O) \frac{e^{-ik\rho}}{\rho} cos\theta \, dx_O dy_O \tag{1}$$

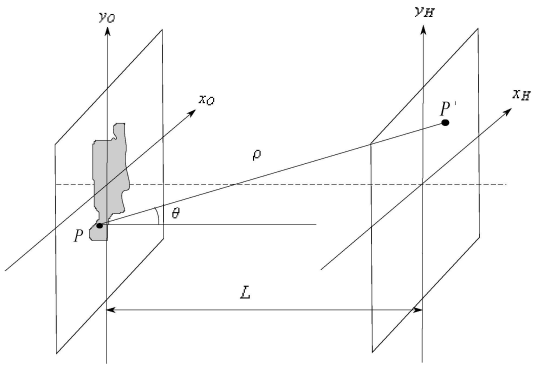

Figure 4: Definitions of object plane, hologram plane, θ, ρ and L.

where

$$\rho = \sqrt{(x_H - x_O)^2 + (y_H - y_O)^2 + L^2} \tag{2}$$

and $E_H(x_H, y_H)$ is the electric field strength in the hologram plane, $E_O(x_O, y_O)$ the electric field strength of the complex amplitude in the object plane, k the wave vector, ρ the distance between a point P in the object plane and a point P' in the hologram plane, θ the angle between PP' and the normal of the object plane and L the distance between the two planes, see figure 4. Equation 1 is then treated further [20]. If the angle θ is small, the paraxial approximation can be used. Since the beam is divergent in our case, this approximation cannot be used as it is. A third plane, called the far field, which is at a large distance from the other two planes, is introduced. The paraxial approximation can then be used between the far field plane and the object or hologram planes. Fast Fourier Techniques are used to integrate equation 1. The harmonic beam is approximated by a Gaussian profile.

Using an in-line setup has some drawbacks. An important one is that the reconstructed object is aligned with a distorted real image, a "twin image" of the object. The twin image owns the same amplitude but opposite phase shift with respect to the wave from the object. There will therefore be an unfocused image superimposed on the focused image. The reason that this problem does not occur in off-line holography is that the angle between the beams causes the images to be separated. There are, however, methods to eliminate these disturbances. The iteration process [11] has been implemented in Lund previously [13].

The phase, ϕ, of a wave depends on its wavelength, λ and the distance, d, traversed in the medium of refractive index n:

$$\phi = \frac{2\pi}{\lambda} nd \tag{3}$$

Investigating the phase of the field in the object plane can thus give information

about refractive indeces or distances.

2.2 Resolution of Space and Reconstruction of Phase

The aim of the project was to investigate the spatial resolution and the possibility to reconstruct phase by a proper target production. The type of resolution we are interested in here is the one that describes the capability of an optical system to distinguish details of space.

There is both a theoretical resolution limit, R_T and an experimental resolution, R, of space and they are quantities in the reconstruction plane. The finest detectable detail of size R_T corresponds to the highest obtainable frequency which in turn and together with the wavelength corresponds to the largest angle of the beam:

$$R_T = \frac{L\lambda}{s} \tag{4}$$

where L is the distance between the object and the detector plane and s the size of the detector. If the beam diameter, D, is smaller than the detector size, this value should be used instead:

$$R_T = \frac{L\lambda}{D} \tag{5}$$

However, the actual resolution, R, obtained might be different. There are different ways to measure this resolution. But along the lines of Mikkelsen *et al.* [14] the sharpness of an edge is what is searched for. The edge is an edge in the transmission of the object, which can be inferred from the reconstructed field. The upper edge is averaged and so is the lower. The width of the central 60 % between these edges is the sharpness and the resolution.

When this holography experiment was run before, a spatial resolution of 4.3 μm was obtained [20]. What was measured was the full width at half maximum (FWHM) of the profile of a tungsten tip, after one shot ("single-shot imaging"). When the hologram was averaged over several images ("multi-shot imaging"), in this case over 200 images, the width of the profile was 4.7 μm.

If one can create objects with sharp edges and look at these, one can work out the actual spatial resolution. Another, natural and complementary, way of looking at spatial resolution is simply to say that is about how small the smallest object that can be distinguished is. Creating objects of different sizes is then also desired. One could also here try to get an object with a varying distance between parts of the object. In studying the spatially resolving capabilities of the setup, one can use objects that do not transmit any light. These objects are referred to as "amplitude objects". The result of studies of the spatial resolution would be quantitative; you end up with a number.

The method has already been used to reconstruct the amplitude of the electric field at the object plane. However, it has never been used to reconstruct the phase of the electric field. To do this is one of the current objectives. One would then look at a"phase object", an object that transmits radiation but changes its phase. An object can only change the phase of passing light compared to the phase of light passing beside it, by having a different refractive index, n, than its surrounding. That means that one should try to make an object with

a refractive index different from 1, the refractive index of vacuum, and compare the phase over the plane just after the object and its surrounding.

In searching for the right material for the phase object it is useful to consider the concept of susceptibility. It describes how a dielectric medium polarizes in response to an electric field [17]. A dielectric medium is an insulator that may be polarized by the action of an applied electric field [8]. The susceptibility of a medium determines its electric permittivity: how an electric field affects, and is affected by, the medium. Related to the fact that the polarization of a material does not respond instantaneously to an applied field, is the concept of complex susceptibility. The real and imaginary parts are connected by the Kramers-Kronig relations [17]. In relation to this a complex refractive index, $\tilde{n}$ can be introduced:

$$\tilde{n} = n + i\kappa \tag{6}$$

The real part n is the ordinary refractive index, the property of the material affecting the phase of a wave. κ can be seen as an extinction coefficient, which describes the amount of intensity lost due to absorption in the medium. An ideal phase object consists of a material with an n very different from 1 and a small κ.

2.3 Targets

Testing the resolution of space and the capability to reconstruct phase of the method includes three necessary steps:

- The processing of objects.
- The characterization of the objects.
- The application of the objects to the holographic setup.

The characterization is essential, since it must be known what has been processed. But before actually executing these steps, a proper design has to be chosen. This affects the choice of processing method and the characterization method.

2.3.1 Choice of Target Design

From the previous parts in this section it seems that the requirements for the object production are:

1. To make objects with sharp edges and preferably with corners.
2. To carefully vary the distance between objects.
3. To make several objects in different sizes that can be studied in one image.
4. To be able to vary the size of the objects between around 50 μm to 100 nm.
5. To make objects that change the phase of the light (of 38.1 nm) and at the same time do not absorb too much of it.
6. To be able to vary the thickness of the object.

7. To be able to vary the refractive index of the object.

8. To be able to mount the object in the holography setup.

2.3.2 Choice of Processing Method

The desired size of the object does not easily fit with requirement 8. Structures of a size of around 1 μm are not so easily mounted. They most likely need to be attached to something bigger. This thing should be fairly transparent for the used wavelength.

A 20 nm thin silicon nitride (Si_3N_4) membrane has in theory a transmission of 33 % for this wavelength [9]. This is to be considered as fairly high. If used it is, however, important to test it in our setup.

Membranes (or "windows") like these are used for transmission electron microscopes and are therefore produced in a fairly large scale and are quite easy to get hold of. The ones used here are 0.5 mm x 0.5 mm and supported by a silicon frame of thickness 0.2 mm and approximately 2.6 mm x 2.6 mm in size, see figure 5, which shows an image taken by a scanning electron microscope. "Membrane" or "Window" will in this report refer to either just the actual

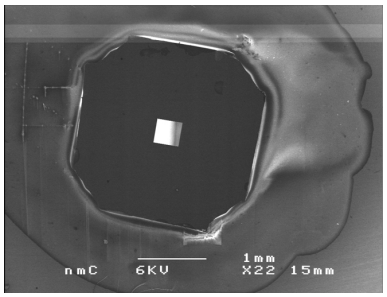

Figure 5: A silicon nitride membrane with its frame.

silicon nitride thin membrane or to the whole piece, including the frame. The membranes are produced by SPI Supplies, who also provides an image of the backside of one, see figure 6.

Fortunately, the membrane reflects some light, so it can fairly easy be seen that a membrane is present in an optical microscope. Figure 7 shows the gray area typical for a whole window. A broken window can be identified on its black color and the pieces of membrane that often stays on the edges of the square hole, see figure 8. Using the dark field mode of the microscope (section 2.3.3) shows these edges even better, see figure 9. It is even possible to tell the difference between a whole and broken window by eye, due to the small reflection.

In order to make an object, one could think of dropping nanowires onto the windows, attaching thin graphite layers, using dust particles and many other things. The requirements of sharp edges, easily controllable size in the range of 50 μm-100 nm, easily controllable distances between objects, however, excludes these possibilities.

Instead, microlithography is a promising possibility. It offers an extreme control. Mirco- or nanolithography is often performed to process devices like micro- and nanochips. In the production of these, a low level of contamination is

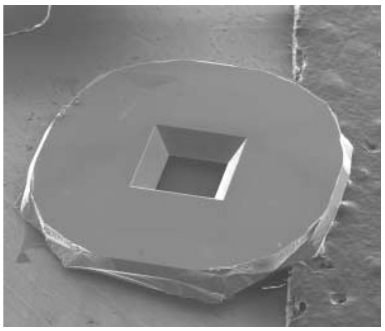

Figure 6: A silicon nitride membrane in the middle surrounded by its frame viewed from the back.

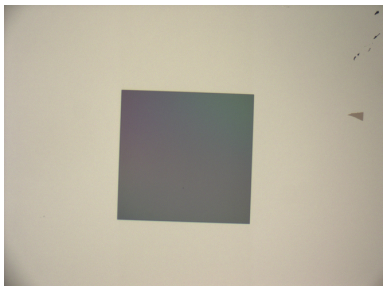

Figure 7: An image of a typical whole window.

crucial. Otherwise, dust particles could settle on the semiconductor wafers (thin discs made of crystalline material) or lithographic masks and cause defects in the devices which result in circuit failure [22]. Therefore, lithography is performed in so called "clean rooms". A clean room is a volume where the level of contamination is controlled. "Microlithography" refers to lithographic patterning methods capable of making features smaller than 10 μm. With nanolithography, one makes structures smaller than 100 nm [8]. But what kind of lithographic patterning methods are there? One can use photolithographic technology, which commonly is used in fabrication of integrated circuits [22].

There is also, among many techniques, electron beam lithography (EBL), that offers a higher pattern resolution, sometimes down to a few nanometers.

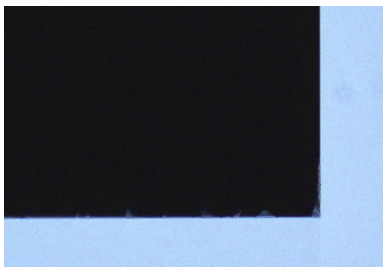

Figure 8: An image of part of a typical broken window.

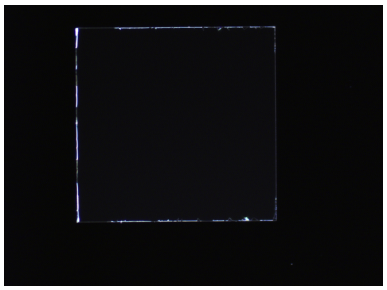

Figure 9: A dark field image of a typical broken window.

The wavelength of a particle is related to its linear momentum, $p = mv$, by

$$\lambda = h/p \tag{7}$$

[2]. If electrons are accelerated from rest by a potential difference V, their kinetic energy K is (assuming that their speed is much less than the speed of light)

$$K = p^2/2m = eV \tag{8}$$

Combining equation 7 and 8 and assuming that the potential difference is 20 kV, yields that the electronic wavelength of these electrons is 0.009 nm. The wavelength of ultraviolet light, used in photolithography, is much longer. As seen in equation 4, the resolution is proportional to the wavelength.

EBL is primarily used to produce photomasks for optical lithography [22]. It is also used in production of and research on nanowires. The flexibility in making a pattern is greater than for optical lithography. The EBL process is about creating a mask. Metal is then evaporated and the mask removed so that there is metal where the mask did not protect. Figures 10-15 show how the process would look on our window. The window is covered with a polymer ("resist") during spin coating and then exposed to an electron beam in specific regions. The exposure causes the bindings in the polymer to break. The result is that the exposed parts of the resist are dissolved during development and the unexposed part left intact. After evaporating a metal and a lift-off of the remains of the resist, there is metal only just where the sample was exposed.

Figure 10: The starting point.

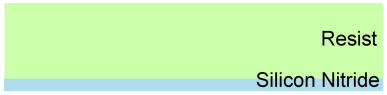

Figure 11: After spincoating.

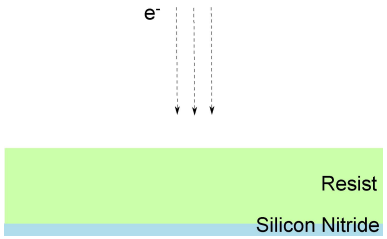

Figure 12: Exposure.

Figure 13: After development.

Figure 14: After evaporation.

Figure 15: After lift-off.

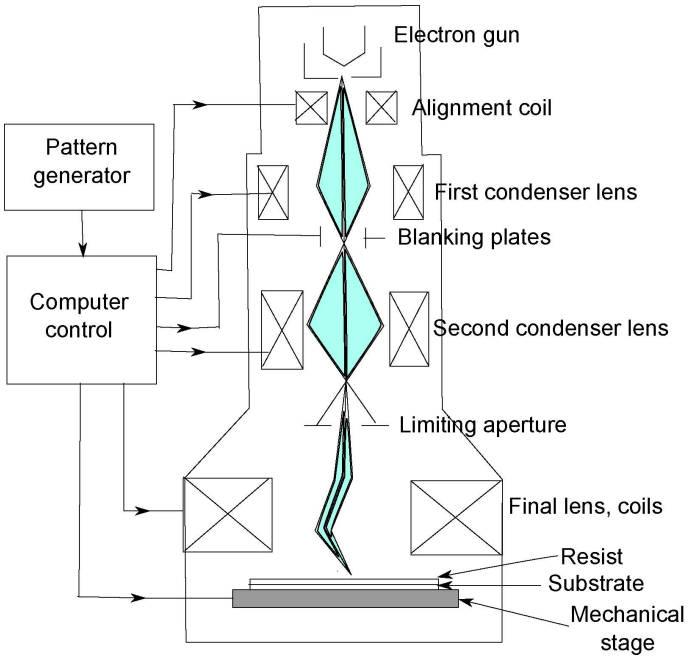

Figure 16: Schematic of an electron-beam machine.

With EBL and evaporation, one can create objects with sharp edges, of different sizes, distances, thicknesses and refractive indeces. This means that amplitude objects and phase objects could be constructed almost the same way. Moreover, due to the possibility of making many types of objects, one can hope that the same procedure can be used also for producing targets that in the future can test the resolution of phase and the temporal resolution of the holographic setup.

What differs between the production of an amplitude object and a phase objects is only the choice of evaporated metal and its thickness. An amplitude object should consist of a metal which is not transparent for the X-UV beam. Gold is an example of a commonly evaporated metal and which has low transmittance at 38.1 nm when it forms a 20 nm thin layer: 4 % [9]. However, gold does not adhere very well to some substrates. One could evaporate a thin, around 5 nm, sticking layer, of for example nickel to the window, and then deposit the gold to solve the problem.

It was seen (section 2.2) that an ideal phase object consists of a material with an n very different from 1 and a small κ. Chromium has a (real) refractive index of $n = 0.689$ and an extinction coefficient κ of 0.1343 for $\lambda = 38.1$ nm [9]. This element seems appropriate for constituting the phase object.

Some general features of how an e-beam machine works is now given [22]. A schematic of an e-beam machine is presented in figure 16. The electron gun can generate a beam of electrons with a suitable current density. In a thermal field emission cathode a current goes through a wire and heats it whereupon the electrons receive an amount of energy Q given by Joule's law. The law states that the generated heat Q depends on the current I passing a wire or foil of

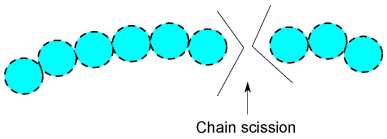

Figure 17: Chain scission.

resistance r during the time t as

$$Q = I^2 rt \tag{9}$$

Because of this energy the electrons can leave the wire and be accelerated in the potential difference. Alignment coils and condenser lenses focus the electron beam to a spot size of 10-25 nm in diameter. Beam-blanking plates turn the beam on and off and a limiting aperture lets only parts of the current through. Beam deflection coils are computer controlled to direct the focused electron beam to any location in the scan field on the substrate. A precision mechanical stage is used to position the substrate to be patterned.

The primary electrons in the incident beam loose energy upon entering a material through inelastic scattering or collisions with other electrons. For a positive resist, the polymer-electron interaction causes chemical bonds to be broken (chain scission) to form shorter molecular fragments, see figure 17. This occurs by electron attachment, which in general can be described as [8]:

$$e^- + AB \rightarrow AB^- \rightarrow A + B^- \tag{10}$$

This reaction is most likely to occur after the electron essentially has come to a halt, since it then is easier to capture. The result of the exposure is hence that the molecular weight is reduced in the irradiated area. This part can be dissolved subsequently in a developer solution - a solution that attacks the low-molecular weight material.

For a negative resist, the irradiation causes radiation-induced polymer linking. The exposed area gets a molecular weight higher than the unexposed areas. The latter can then be dissolved by a developer that does not attack high-molecular-weight material. A positive resist lets the resulting metal structure be of the same shape as the pattern transferred by the beam. The procedure involving a positive resist is what is illustrated in figure 10-15 and is preferable in the present case.

When an electron enters the resist positioned on a substrate, it travels in the resist and finally, when all energy is lost, it stops. It can also go through the resist, enter the substrate, undergo collisions here and scatter back into the resist. The effect of the back scattered electrons is that the developed pattern is wider than the scanned pattern. The effect is known as the "proximity effect". It depends on beam accelerating voltage, resist material and thickness, substrate material, the resist contrast characteristics (how the solubility of resist depends on "dose") and the chemical development process used [4]. In tests performed using a 25 kV beam, back scattered electrons was causing 20 to 30 % of the total exposure [4]. The zone of exposure introduced by the backscattered electrons was approximately 2-3 μm in radius. Apart from the parameters mentioned, it is also likely that the thickness of the substrate affects the back scattering. If very thin, the electrons could go straight through it.

Figure 18: Electron trajectories. The electrons travel straight through the higher PMMA layer and hit the lower Silicon Nitride membrane. No electrons are scattered back to the PMMA.

Trajectories:	100
Beam energy:	20 keV
Beam shape:	Gaussian
Beam radius:	4 nm
PMMA, thickness:	100 nm
Si_3Ni_4, thickness:	20 nm
Si_3Ni_4, atomic number:	70
Si_3Ni_4, atomic weight/g/mol:	140,2833
Si_3Ni_4, density/g/cm^2:	6,905004

Table 1: Trajectory parameters.

For the present case, where a very thin, 20 nm, substrate is considered, this has some bearing. Most likely the share of back scattered electrons will be smaller than with a normal, thicker, substrate. One can look at a Monte Carlo simulation of trajectories in our sample. The parameters used are given by table 1.

In the simulation, no electrons are backscattered. That suggests that more charge is needed for a given area, in the case of a thinner substrate like the window, than when using a thicker substrate, in order to get the same exposed pattern. The deposited charge per area is referred to as "dose". The dose depends on the acceleration voltage, the type and thickness of the resist, the developing method, and substrate material and thickness. To perform a dose test is advisable. The aim of using a beam of electrons and developing was to remove resist in certain areas - where a metal structure is desired. The aim of the dose test is to search for a dose such that the exposed areas are completely empty of resist but intact in shape, after development. Underexposing means leaving a small layer of resist in the exposed area, whereas overexposing means that the amount of charge has changed the shape of the pattern.

Looking at the spin coated sample in the electron microscope of the electron beam machine affects the resist. Therefore, one cannot look through this microscope and search for a good spot to make the exposure on. One can only look at less important areas, where a damage of the resist does not cause problems. This is usually the edges of a sample. In order to then make the exposure, one has to know the distance from the edge to the area desired to expose with the electron beam. The fact that the sample is bombarded with electrons also has other effects. The sample should be as conducting as possible, so that charge

Figure 19: Metal sticking to the sides of the resist.

does not build up and distorts the image.

The resist suitable for the present procedure is 950 poly-methyl methacrylate (PMMA), where "950" stands for a molecular weight of 950.000. It is often dissolved in anisole, constituting around 5 % of the mix. The mix of a concentration of 4% 950PMMA in anisole is referred to as "950PMMA A4". One developer that dissolves it is methyl isobutyl ketone mixed (MIBK) with isopropanol (IPA). MIBK is the active ingredient, the solvent. It attacks and resolves the parts of the PMMA whose molecular weight has been reduced due to chain scissions. If there are still remains of resist at exposed areas after development, one can bombard the sample with plasma. This will decrease the height of the resist and thereby remove the unwanted remains.

Acetone then completely resolves all the PMMA after evaporation, in the lift-off process. To ease the lift-off process, the resist must be thicker than the metal. If the resist is thin, metal vapors that stick to the side of the resist could connect the metal layer that is undesirable with the desired structure, see figure 19. With a thicker resist the metal on the side of the resist is more spread out and this effect is less likely. This reasoning might be of extra importance when dealing with the membranes. The effect of the surrounding metal piece being attached to the wanted structure might in our case be that the whole window, or pieces of it, is removed together with the wanted structure. For the present attempt to create structures, it might therefore be reasonable to have a resist thickness - metal thickness - relation which is 3:1, or more. Since the membrane is so thin, it seems wise to also make a fairly thin metal structure on it. If one wants to make a structure of thickness 20 nm, the resist thickness should be at least 60 nm.

The desired thickness of the resist is obtained by spinning the substrate (hence the name "spin" coating) at a certain speed. The curve in figure 20, provided by the resist manufacturer, shows how thickness depends on speed for three concentrations of PMMA [10]. However, these curves were based on measurements for larger substrates. The fact that our sample is so small can have unpredictable effects on the profile of the resist.

When illuminated, the resist will shine in bright colors. The color of the resist depends on which wavelength that suffers destructive interference [2]. This destructive interference is, under some conditions, due to that the optical path difference between the light reflected at the resist surface and the light coming up to the surface after reflection at the resist bottom is equal to an integer of the wavelength. In this situation, the phase difference is π, since such is introduced for the wave reflected at the resist surface. The colors seen in thin films are not monochromatic. They are called "subtractive" colors since the apparent color is determined primarily by what is missing from the reflected

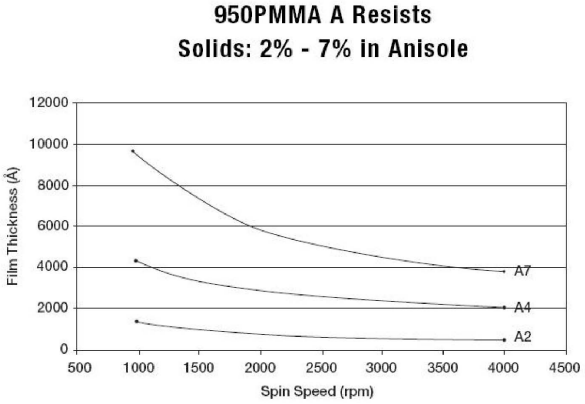

Figure 20: PMMA speed curve.

light [2].

Evaporation is about depositing a thin metal film. When a source is heated above its melting point in an evacuated chamber, evaporation occurs [22]. The atoms then travel at high velocities in straight-line trajectories. One way to heat the source is by resistance heating, where the produced energy is given by Joule's law, equation 9.

The substrate used in EBL and the evaporation process is almost always a lot thicker and harder than the silicon nitride membrane that is preferable to use in the present case. Typically, silicon wafers of thickness around 300 μm are used when dealing with nanowires. These are not sensitive to the steps involved in the EBL- and evaporation process. It is unclear whether the windows can survive the steps. However, the amount of control obtained by using EBL and evaporation speaks for exploring their possibilities. And, EBL and evaporation was accomplished on 200 nm membranes in 1998 by M. M. Leivo and J. P. Pekola [12]. Additionally, it is not unlikely that a successful result here could have influence on other projects than digital holography. It is interesting in itself how well it works to create structures by this technique on such thin membranes.

2.3.3 Choice of Characterization Method

When it comes to the characterization of the built objects, there are two natural options: the optical microscope and the electron microscope. An optical microscope uses visible light and a system of lenses to magnify images of small samples. In a compound microscope, there are two major parts to the microscope, an objective and an eyepiece, or ocular lens [2]. The objective places an enlarged image of the object at a point closer to the eyepiece than its focal length. The eyepiece than acts as a magnifier. Samples can be observed by two types of illumination techniques, bright field and dark field. The bright field illumination technique is the common one. A dark field microscope blocks the light that transmits the sample and only light scattered from the object forms an image, see figure 21 [8]. This causes edges to be clearly seen.

Electron microscopes use a beam of electrons to illuminate the sample and

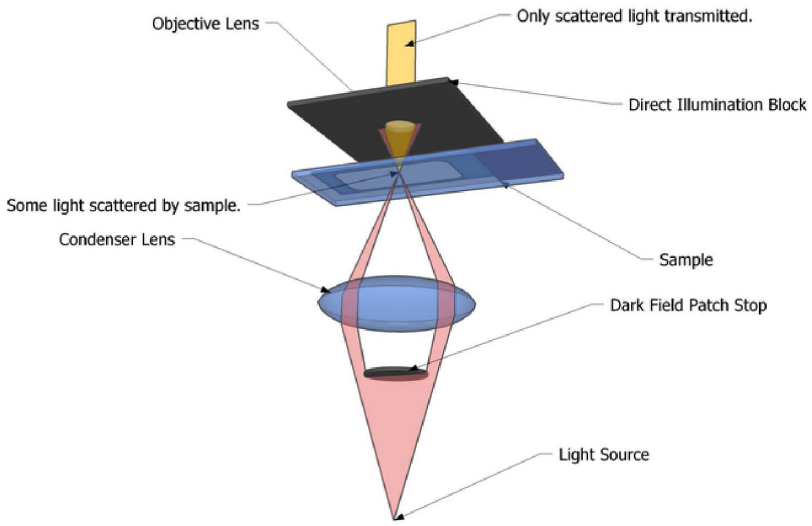

Figure 21: A dark field microscope.

create a magnified image of it [21]. Its resolving power is better than that of an optical microscope, since the wavelength associated with electrons are shorter than the wavelength of photons, equation 4. This allows for a far higher effective magnification. Their operation is similar to that of the e-beam machine. In fact, many e-beam machines are electron microscopes connected to a pattern generator. The electrons in the microscopes are produced by an electron gun and directed by a series of electromagnetic lenses. The condenser lens collimates the electron beam on the sample and an enlarged image is produced by a series of magnifying lenses. Since the electrons can travel only in a high vacuum, the entire path must be evacuated. There are different types of electron microscopes: scanning-, transmission-, reflection-, scanning transmission- and low voltage-electron microscopes.

The scanning electron microscope (SEM) permits the observation and characterization of organic and inorganic materials on a nanometer scale [7]. Its popularity stems from its capability of obtaining three dimensional-like images of the surfaces of a wide range of materials. The type of signals produced from the interaction of the electron beam with the sample include secondary electrons, backscattered electrons, characteristic x-rays and other photons. The secondary and backscattered electrons are the imaging signals of greatest interest. The reason is that these vary primarily as a result of differences in surface topography. The three-dimensional appearance of the image is due to, among other things, the large depth of field of the SEM.

The more detailed image speaks for using an electron microscope as well as an optical. The optical microscope is quicker to use and suitable for checking the status of the sample during the processing. The resulting structures are preferably characterized by an electron microscope.

Figure 22: The window with frame glued with indium to a support structure.

3 Target Processing

The electron beam lithography and evaporation is performed in the Lund Nano Lab. The part of the lab where the EBL is performed is an ISO 5 clean room environment: there are only 3 520 particles bigger than 0.5 μm per cubic meter. In a typical urban environment there are 35 000 000 such particles in this volume [8]. For the present experiment, however, the cleanliness in itself it is not of great importance. A dust particle on the membrane does not stop us from using it. But there is one great advantage in working in the Lund Nano Lab: that the temperature and humidity is kept constant. This enables one to develop a "recipe" for the EBL process, including steps whose outcome might be temperature or humidity dependent, that will always work.

3.1 Preparation

Since the windows are so small, approximately 3 mm including the frame, they need to be attached to something bigger in order to be handled in the processing steps. As they are, they cannot be used in the holography setup either. They are glued with indium melted on a hot plate onto a rectangular support structure made of stainless steel. This structure is 2 cm long, 1 cm high and 0.8 mm thick, see figure 22.

It is important not to get any indium on the bottom side of the support structure, as this seems greatly to obstruct the process of applying resist onto the window, the spin coating.

Indium was chosen instead of baked (20 min, 180 °C) silver glue as this was seen to dissolve in acetone and greatly contaminate the window, see figure 23. The membrane is glued onto a hole in the structure so that light can go right through the window and the hole. If the support structure like this were attached to something and the surrounding pumped for vacuum, there would be air kept in a pocket underneath the window. This could cause the window to break. Therefore, an escape route for the air is made, in the shape of a track leading away from the hole on the bottom side of the support structure. There is also a hole for attaching the support structure to the stage in the holography setup. The membrane is inspected in an optical microscope between every step. This way it is made sure that it is whole. Cleaning the window involves putting it in a beaker of acetone for a few minutes, lifting it while keeping it wet into a

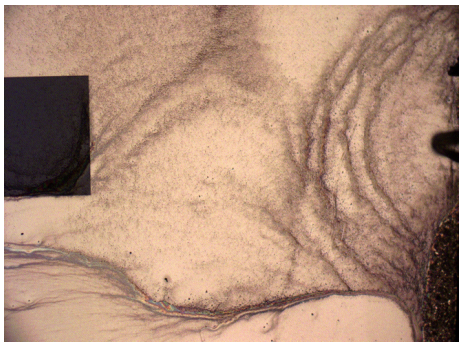

Figure 23: Contamination of silver glue.

beaker of isopropanol where it should rest for a minute or so. It is then taken out of the beaker and dried with gas from a nitrogen gun. Acetone removes organic particles effectively. However, it leaves stains behind when it evaporates. This is why the sample has to be kept wet with acetone the whole time until it is put is isopropanol, which leaves less marks during evaporation. Blowing the sample gently from the side with a nitrogen gun will enhance the evaporation and decrease the tendency for leaving marks.

If the window is not too dirty, the cleaning process could be skipped, as it increases the risk of damaging the window. Dropping the support structure when it is in liquid easily breaks it. Also, the balance between managing to dry the sample by blowing nitrogen on it and not breaking it is a little bit problematic. Due to carefulness, stains are often left on the window after the cleaning process.

3.2 Spin Coating

During the spinning, the substrate is fastened to a rotatable chuck by the effect of a vacuum pump. The holes in the available chucks of the spinner are all placed in the middle of the chucks and are of at least 2-3 mm in diameter. This is one of the reasons that a support structure for the window is necessary; the window is simply too small for the hole, and the membrane would break if placed on the hole, due to the vacuum. Since just underneath the membrane there is a hole in the support structure, one cannot place this part on the hole and in the center of the chuck. Applying the support structure directly onto the chuck forces oneself to spin the sample in an off-axis way.

Having tried this and seen that the spread of the resist turned out quite unevenly, another solution was found, see figure 24. The support structure is glued onto a 2 inch silicon wafer which can be attached to the chuck. The wafer is first fastened at the chuck. 950PMMA A6 is applied. The wafer is then spun at 1000 rotations per minute (rpm), so that the resist evenly spreads out. The support structure is then placed on the wafer so that the window is at the center of the wafer. The wafer with the support structure is then placed on a hot plate at 180 °C for 10 minutes. This causes the resist to act as a glue which effectively holds the support structure on its place on the wafer. If there is indium on the bottom side of the support structure, the gluing is obstructed.

The wafer is then placed on the middle of the chuck, so that the window

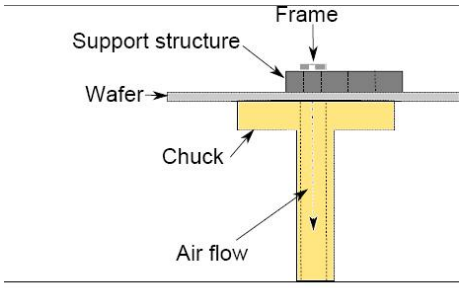

Figure 24: The support structure is fastened to a wafer which can be held at the chuck.

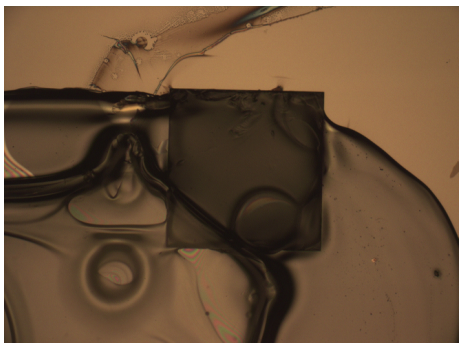

Figure 25: Resist from the wafer beneath on a window frame.

too is approximately in the center here. This construction can handle spin speeds up to 3000 rpm. Also, the outcome of spinning just the *wafer* slower, at 200 instead of 1000 rpm for 45 seconds in order to increase resist thickness and maybe gluing ability, was observed. The result was that the resist bubbled through the window from below and hence broke it, see figure 25 which shows resist on the window frame coming from the window hole. Failing attempts were made to glue the support structure by resist to a smaller 1 inch wafer.

950PMMA A4 is applied by a pipette onto the actual frame. It is not dropped directly onto the window, but it is made sure that the resist covers the window before spinning. The chuck is spun according to table 2. This speed would according to the curve in figure 20 yield a resist thickness of around 190 nm.

Time/s	Acceleration/rpm/s	Speed/rpm
10	300	400
45	1500	3000

Table 2: Spinning recipe.

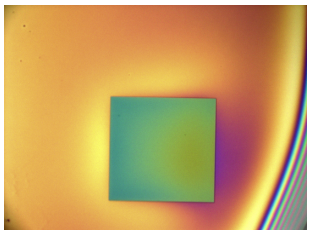

Figure 26: Sample "Spatial1" spin coated.

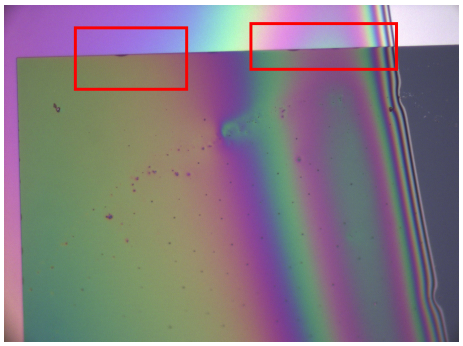

Figure 27: "I" spin coated. What might be mistaken as rests of a broken window are marked.

Figure 26 shows sample "Spatial1", after it has been spin coated. The green square in the middle is the window. Usually the color of the window is fairly uniform. After the spin coating, the wafer is put at a hot plate for 10 minutes at 180 °C. This removes the solvent from the resist film and makes the resist solid. The resist adhesion to the window improves this way and the later exposed patterns will stay fixed.

When inspecting the sample in a microscope at this point, one might get the impression of a broken window underneath the resist, see figure 27 presenting sample "I", where parts that might be mistaken as remains of membrane are indicated. However, another image of "I" taken shortly after the image in figure 27 strongly indicates, by the way the window was broken, that the parts looking like remains of membrane was not, see figure 28. A small scratch, around 1 mm in length, is made in the resist, starting from the lower edge of the frame. This scratch can be used for adjusting a good focus in the electron beam machine.

Tests of spinning 50 nm windows more precisely placed at the center of the spinner gave a different resist profile than the 20 nm windows spun just approximately in the center. The result was a colorless resist layer right on the window, and a small "blob" of resist gathered to the side, mostly on the frame.

This process is performed to produce Spatial1, Spatial2 and Phasial. There were also attempts to spin coat windows of a thickness of 50 nm.

3.3 Exposure

Before put in the electron beam machine, the spin coated window is inspected in an optical microscope. The distance from a point at the lower left corner of

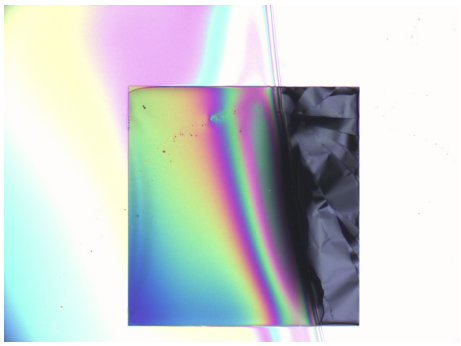

Figure 28: "I" when the membrane is broken. The way it is broken strongly indicates that what before looked as remains of membrane were not.

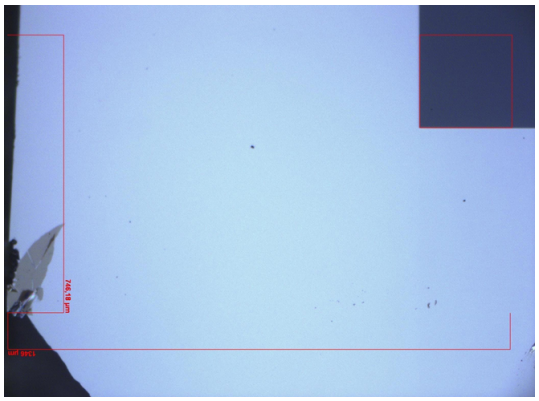

Figure 29: An example of a coordinate system.

the frame to the center of the membrane is measured, according to the example in figure 29. If the position for the chosen origin can be found in the electron microscope, this can be chosen as the origin for the patterning and one can use the coordinates of the window center position from the optical image. For this to work however, the coordinate system of the electron beam machine must be in angular agreement with the coordinate system of the optical image. The window is placed so that the axes of the coordinate system is parallel to the window axes, see figure 29. On some samples the lower edge of the frame is parallel to the higher and lower frame of the window. Two points on this edge can then be used to define one axis, and hence both axes since they are perpendicular. Hence the electron beam machine- axes are parallel to the axes of the optical image. If the lower frame axis is not parallel to the window edge, one has to find two other points such that a line connecting them are. These two points are then used in the e-beam machine system to define the axes. Figure 30 shows a resulting image, after the search for the chosen origin along the edge and after development.

The electron gun of the e-beam machine in Lund has a thermal field emission cathode that produces the free electrons. The e-beam lithography system consists of a SEM integrated with a pattern generator. The pattern generator is what effects the otherwise raster scanning beam to move according to the

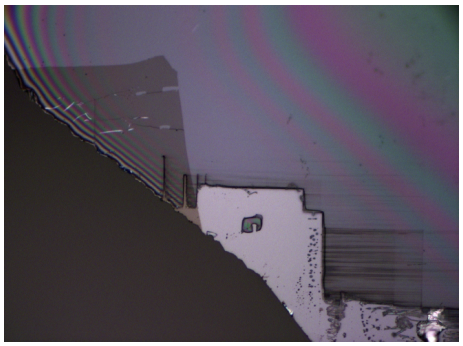

Figure 30: Areas where resist has been removed due to search for the origin along the edge of the frame.

Figure 31: The e-beam machine at Lund Nano Lab.

desired pattern. Raster scanning means scanning a whole area systematically, line by line. That this is done by the SEM can also be seen in the previous figure 30, where whole rectangular pieces of resist are missing.

In figure 31, showing a photo of the e-beam system in the Nano Lab, the SEM is to the left. It is protected by sound proof walls to minimize vibrations. The pattern generator is in the middle of figure 31. The SEM is controlled by the computer connected to the right screen whereas the left computer is running the Raith150 software where the exposure pattern is made. The e-beam machine creates a beam of spot size 20 nm. The machine uses a vector scan for the writing. This means that the beam is directed only to the requested pattern features and jumps from feature to feature, rather than scanning the whole so called write field, as in raster scanning.

An acceleration voltage of 20 kV and an aperture of 10 μm is used for the present processing of Spatial1, Spatial2 and Phasial. A dose test is made, where the dose is varied between 150 and 360 μC/cm^2. Figure 32 shows a bright field image of the sample with the dose test. Some traces of resist can be seen in the first rectangle on the window in these two lower rows. Figure 33 shows the same but this time the image is taken in dark field mode. In this image the resist traces are prominent. It was found that a dose of 340 μC/cm^2 worked well for a substrate of silicon nitride of thickness 20 nm for the slightly varying resist thicknesses that occurred.

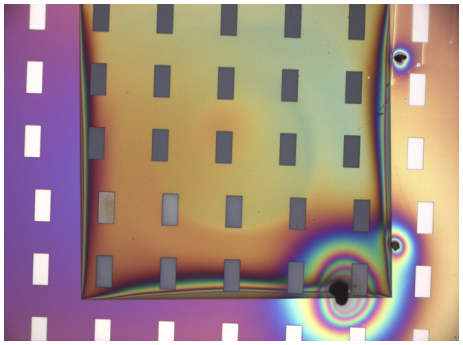

Figure 32: Dose test, bright field image.

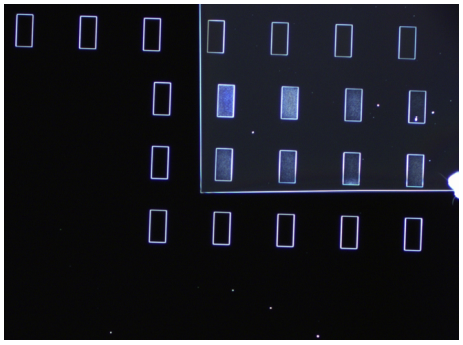

Figure 33: Dose test, dark field image.

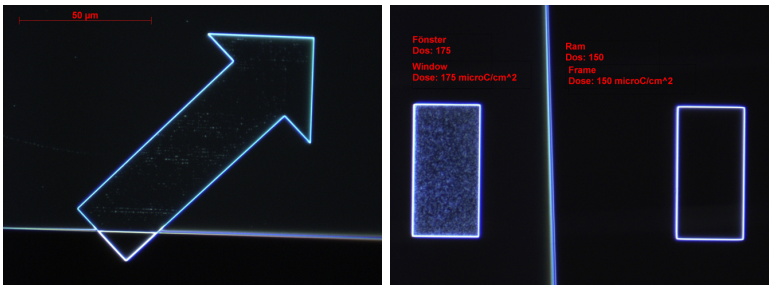

Figure 34: (a) An arrow covering frame (underneath the horizontal line) and window (above horizontal line) after development. (b) Two rectangles after development. The left one is situated at the window and has been made with a dose of 175 μC/cm^2. The right is made at the frame and with a dose of 150 μC/cm^2.

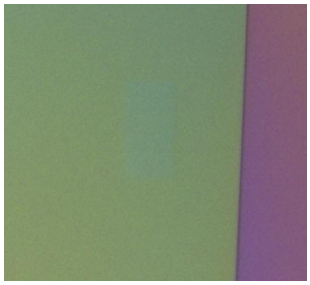

Figure 35: Sample "Spatial1" after exposure.

Differences between the amount of resist left-overs on the window and such left-overs on the frame could be found, see figure 34. Both images are taken after development. In figure (a) the bottom of the arrow is situated outside the window, on its frame. One can see that here are no remains of resist. However, on the actual window, that is above the horizontal line, there are left-overs of resist. In figure (b), the left rectangle is situated at the window and the right one at the frame. A dose of 175 μC/cm^2 was used for the left and 150 μC/cm^2 for the right was used. Hence, although a higher dose was used on the window than on the frame, less resist was removed.

The result of a dose test on the 50 nm windows was that a dose of 340 μC/cm^2 was not enough to fully remove the resist in the exposed areas.

Figure 35 shows Spatial1 after part of it was exposed in a rectangular fashion. The almost invisible rectangle is exposed on the window and the edge of the window is the vertical line to the right.

Spatial1 is exposed so that there are many sharp edges and corners, and so that it contains objects, squares, of different sizes. Spatial2 is exposed so that it gets sharp-edged structures whose distance vary. The phase object is exposed so that a rectangular structure can be made. Exposure is also tried on the 50 nm windows.

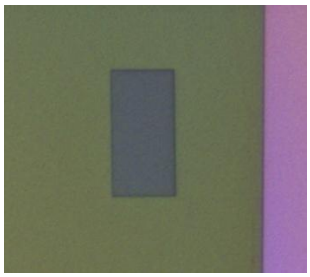

Figure 36: Spatial1 after development.

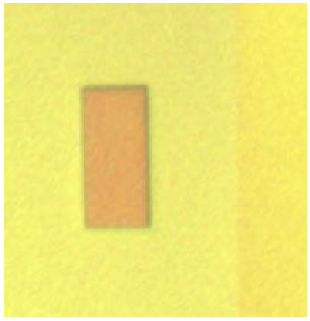

Figure 37: Spatial1 after evaporation.

3.4 Development

The developer used is MIBK:IPA in the ratio 1:3. The window on its support structure is placed in a beaker of this developer for 1 minute and 30 seconds. It is then placed in a beaker of IPA for rinsing for 30 s. Figure 36 shows the same rectangle on Spatial1 as figure 35 after development. Here the gray surface of the membrane can be seen at the bottom of the rectangle. Sample Spatial2 is bombarded with plasma, due to problems with exposure.

3.5 Evaporation

Our windows are evaporated on by resistance heating. The available metals are placed in so-called "boats" that lead current. Heated by electric power the chosen metal evaporates. The pressure in the chamber is less than 10^{-6} mbar. A thickness meter measures the thickness of the deposited metal film.

Spatial1 and Spatial2 is made by evaporating 20 nm gold onto the windows. Figure 37 shows the rectangle on Spatial1 after the sample has been evaporated on. An example of gold not sticking well to silicon nitride was obtained and is presented in figure 38. The golden rectangle in the middle was not evaporated where it is in the image, but moved there during lift-off.

Phasial is made by evaporating 27.6 nm of chromium. This gives an expected phase difference of 1.4 radians between the field by the object and the field around (equation 3). The chromium used did not, as was the case for gold, form a uniform film after evaporation. It was quickly filled with small cracks at the resist surface but uniform at the exposed area, see figure 39.

The 50 nm windows are evaporated by 5 nm nickel and 20 nm gold.

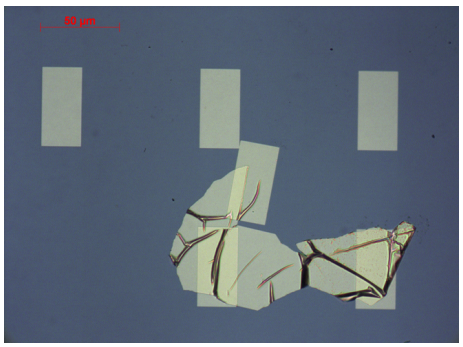

Figure 38: The gold rectangle in the middle has moved.

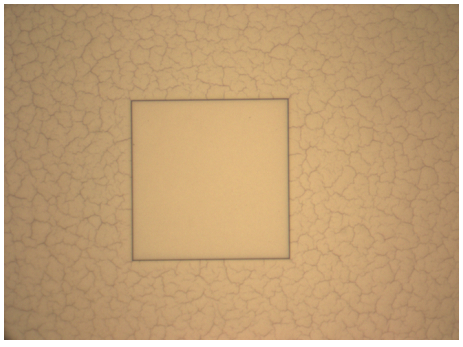

Figure 39: Cracks in chromium covering resist and an even metal layer on the naked piece of membrane in the middle. The center square is the object of Phasial.

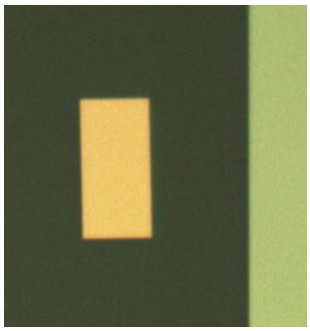

Figure 40: Spatial1 after lift-off.

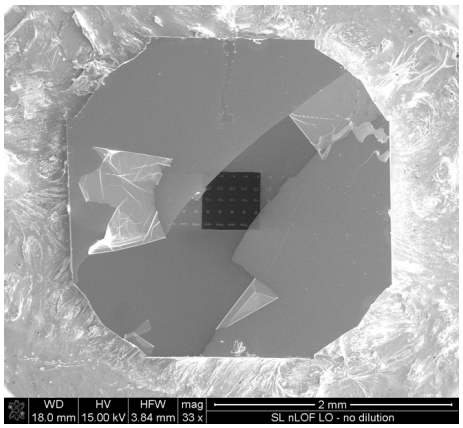

Figure 41: The full frame after lift-off.

3.6 Lift-off

After evaporation the window is placed in a beaker of acetone. The acetone resolves the resist and thereby removes the metal pieces covering it. The metal film sticking to the window stays and constitute the object. The window is then rinsed in isopropanol and gently dried with a nitrogen gun. This process takes anything from a few hours to several days, depending on how well the acetone can reach the resist for the metal layer. Figure 40 shows the rectangle on Spatial1 and surrounding as it looks after lift-off.

An image of the full piece, including the frame, as it can look after the process is given in figure 41. The lift-off was not completely successful on this sample, as a lot of the metal would not come off the frame. However, it was successful on the relevant part, the window.

4 Target Characterization

The type of microscopes used are compound microscopes. The sample is both illuminated and observed from above in the bright field mode. In the dark field mode, the sample is also observed from above and illuminated roughly from above.

Three samples were produced: Spatial1, Spatial2 and Phasial. Figure 42 shows sample Spatial 1. The object contains 5 rectangles and 9 squares of sides

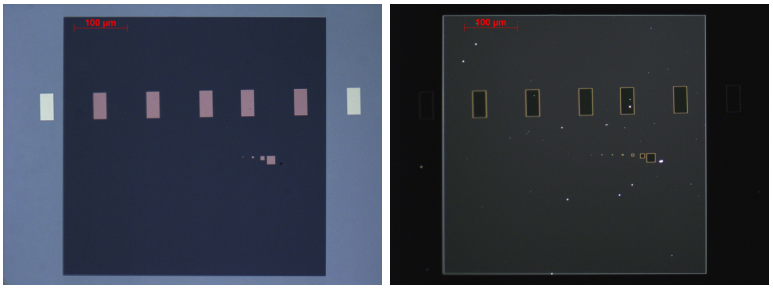

Figure 42: Spatial1 (a) optically imaged, bright field, (b) optically imaged, dark field.

16, 8, 4, 2, ..., 0.0625 μm. Figure 43 shows Spatial2 optically imaged by a) bright field and b) dark field. The upper row contains rectangles of size 30x20 μm, and

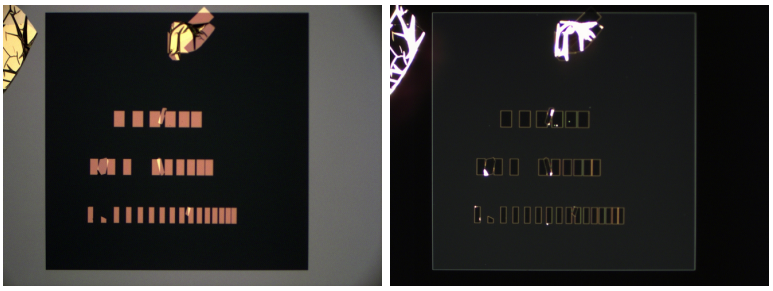

Figure 43: Spatial2 (a) optically imaged, bright field, and (b) optically imaged, dark field.

with a spacing decreasing as 15, 12, ..., 3 μm. The middle row rectangles are 30x10 μm and the distance between them decreases as 15, 13, ..., 1 μm. The last row rectangles are 30x10 μm and their distance decreases as 15, 14, ..., 1 μm. A misplaced arrow (the structure at the top of the window) did not survive the lift-off properly. It was to indicate the position of the upper left rectangle.

Phasial is shown in figure 44. The chromium rectangle is approximately 40x45 μm in size. Some gold structures were made on a 50 nm window. Figure 45 shows a SEM image of one of them.

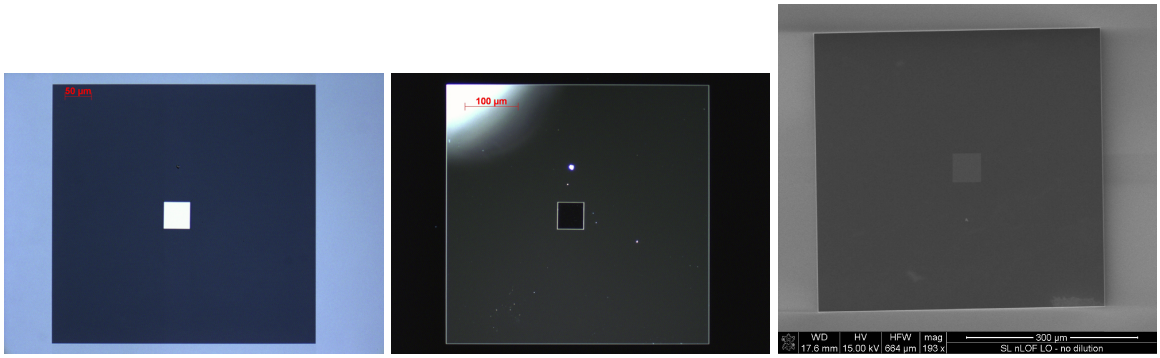

Figure 44: Phasial (a) optically imaged, bright field, (b) optically imaged, dark field and (c) electronically imaged.

Figure 45: A SEM image of a tulip made on a 50 nm window.

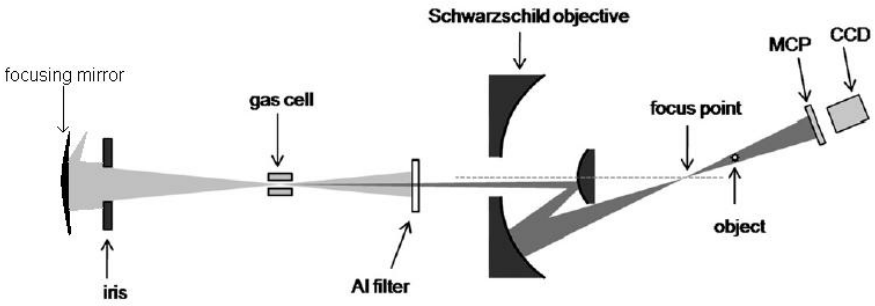

Figure 46: The holography experimental setup.

5 Holography

5.1 Experimental Method

Once the targets have been processed and characterized they are investigated in the holography setup. The setup is shown in figure 46. The incident infrared laser beam at 800 nm is provided by a 40 TW laser system. The laser system is operating at 10 Hz repetition rate and with pulses of a duration of 40 fs. The pulses are focused by a mirror of a focal length of 2 m onto the gas target where the generation takes place. The HHG efficiency is optimized by an iris. The iris clips the beam to a diameter of less than 15 mm. 20 mJ are thereby used for the non-linear conversion.

The gas is filled with argon through a piezo-driven injection system. It is possible to precisely control the opening time of the gas valve with respect to the incoming laser pulse. The harmonic beam created is emitted along the laser axis, with a divergence of 0.4 mrad. A 205 nm thin aluminum filter blocks the infrared radiation. The beam is focused by a Schwarzschild objective about 2 m from the gas cell. The objective contains two spherical mirrors, one concave and one convex. They are centered at the same point. The mirrors are coated to select the 21st harmonic, 38.1 nm.

The focal length of the objective is 26.9 mm. In order to reduce intensity losses the objective is placed off-axis. The focal point is located at a distance of 48 mm behind the objective, and the harmonic beam is divergent with a half angle of 75 mrad. The target is mounted on a motorized translation stage and can be precisely positioned in the divergent beam after the focus point. The scattered parts of the beam interacts with the unaffected parts and an interference pattern is recorded. A mirco channel plate (MCP) records the intensity distribution of the beam. This distance, L, between the object and detector is 315 mm. The MCP is connected to a phosphor screen, imaged by a CCD camera. The beam diameter at the detector, D, is 1 cm. According to equation 5, the theoretical resolution, R_T, is therefore 1.2 μm.

An empty window - a window without any structure on it - is first investigated and its transmission measured. Spatial1, Spatial2 and Phasial are then investigated. When looking at Spatial1, the squares are observed. A large number of background images are taken of each sample, then averaged and sub-

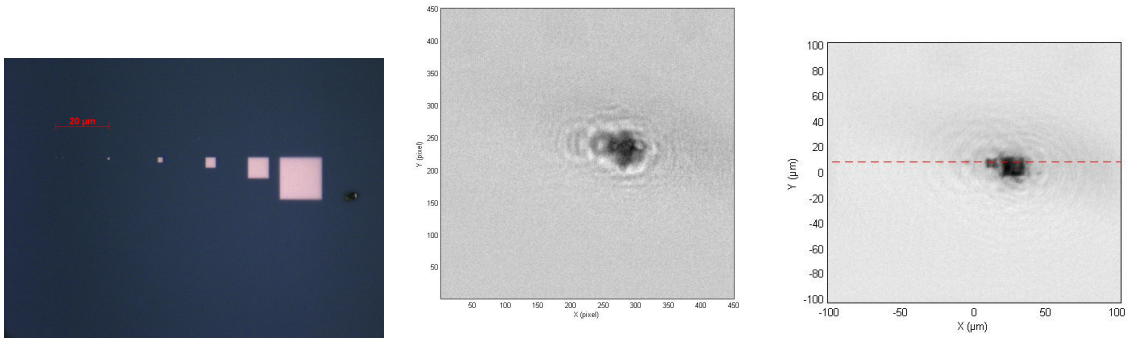

Figure 47: The Spatial1 squares. (a) Optical image. (b) The experimental hologram. (c) The reconstructed transmission in the object plane.

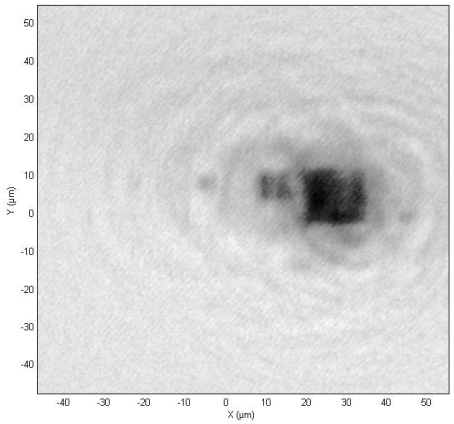

Figure 48: The reconstructed transmission of Spatial1 magnified.

tracted from the image. A reconstruction is made and the iterative process to improve the image quality applied.

5.2 Results

The transmission measured for the 20 nm window was 46 % and 26 % for the 50 nm window. Different representations of the squares in Spatial1 are given in figure 47. Figure 47a shows them optically imaged, figure 47b shows the experimentally obtained hologram and figure 47c the reconstructed transmission of the object. Figure 48 shows the same reconstructed transmission as 47c, but magnified.

The transmission along the line shown in figure 47c is shown in figure 49. The sharpest edge is chosen for calculating the experimental resolution R. The upper edge is averaged and so is the lower. The width of the central 60 % between these edges is then the resolution. The value obtained is 1.45 μm.

The membrane of Spatial2 was destroyed at some point in the application

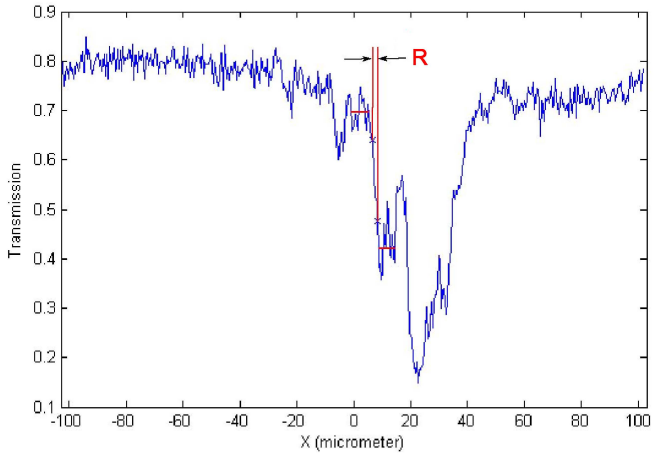

Figure 49: Transmission along the line shown in figure 47c. The experimental resolution limit, R is obtained by calculating the width between an averaged upper and lower edge. It is not the width of the whole slope that is used, rather the width of the central 60 % of the height.

procedure.

Figure 50 shows Phasial electronically imaged and then its hologram. The reconstructed transmission distribution over the object plane is shown in figure 51. The reconstructed phase of the electric field in the object plane is shown in figure 52.

The tulip made on the 50 nm window and its reconstructed transmission is presented in figure 53.

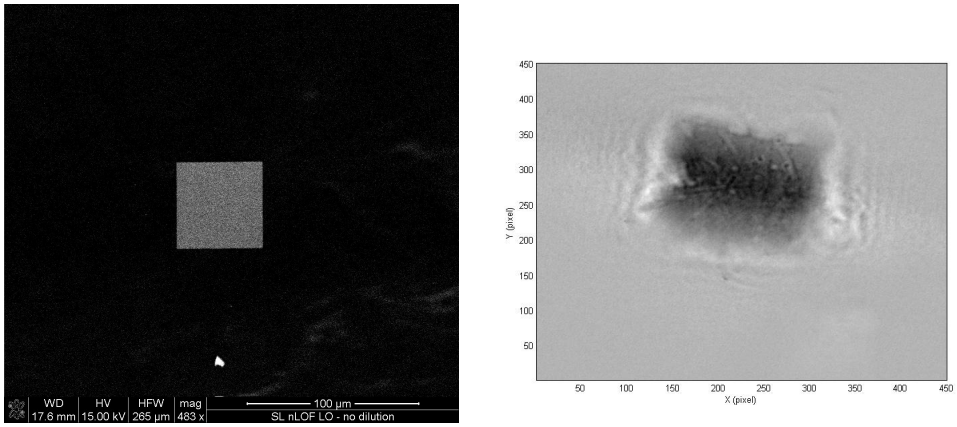

Figure 50: (a)Phasial electronically imaged. (b)The hologram of Phasial.

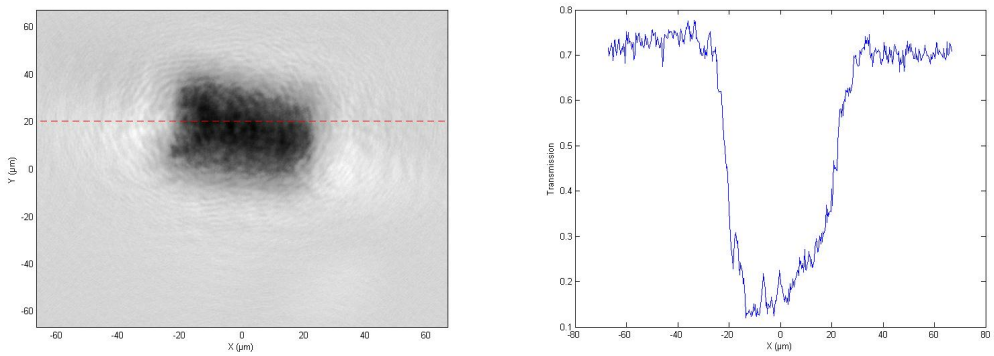

Figure 51: (a)The reconstructed transmission of Phasial. (b)The transmission along the line drawn in (a).

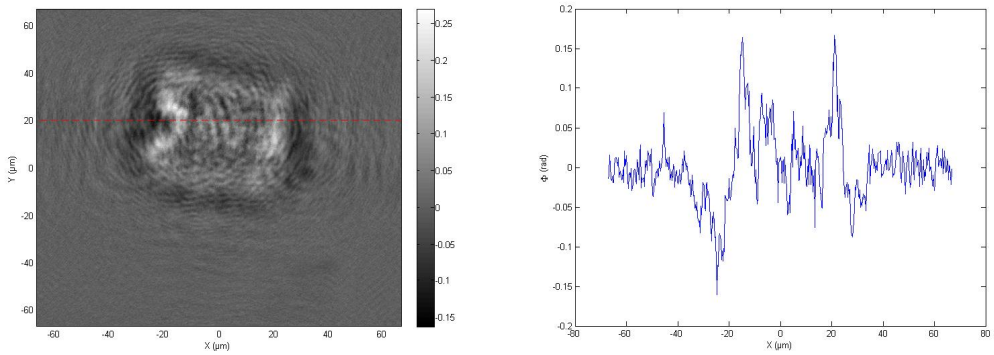

Figure 52: (a) The electric field phase distribution in the object plane. (b) The phase along the line drawn in figure (a).

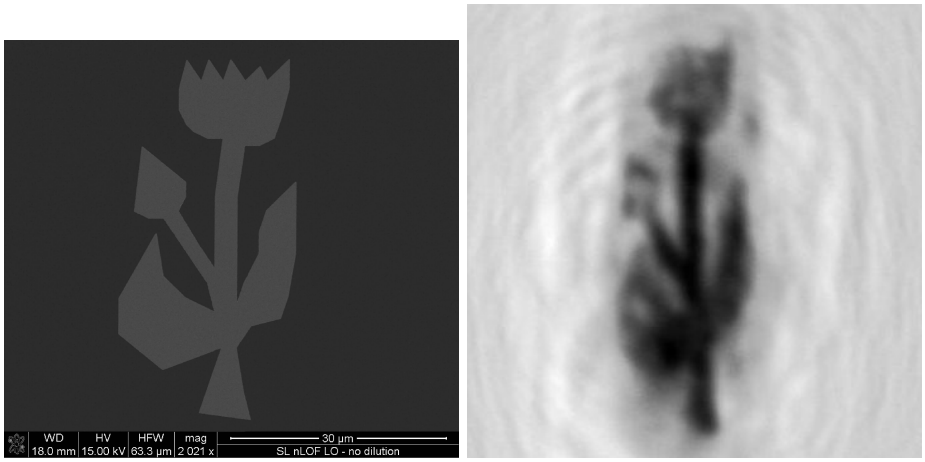

Figure 53: (a) A SEM image of the tulip. (b) The reconstructed transmission of the tulip.

6 Discussion and Outlook

The aim of the project was to measure the spatial resolution of the digital holography setup in Lund and examine its capability to reconstruct phase. Three targets were produced: Spatial1, Spatial2 and Phasial. By this, it was proven that performing electron beam lithography and evaporation on thin 20 nm silicon nitride membranes works.

Some tests seems to confirm what was expected: that a higher dose in the e-beam machine is needed for these thin windows, compared to normal substrates. This seems to have been the case illustrated in figure 34. The reason is the smaller amount of back scattered electrons in a thinner substrate, since more electrons could just continue straight through the membrane. Surprisingly, a bigger dose was needed for the 50 nm windows than for the 20 nm windows. However, it can not be excluded that the resist adhesion is different in their case, and hence that the resist profile differed and affected the dose needed.

Also somewhat surprisingly it seemed inadvisable to be very careful when placing the window just in the middle of the spinner, at least in the case of the 50 nm windows. The result was then often the mentioned small blob, surrounded by an almost transparent resist layer. It might be that the resist did not adhere well in general and that it was only a small part that stayed on the frame. Placing these windows a little bit off-axis, however, seemed to help in getting a resist layer in color, which has proven promising for a good exposure.

Holograms could be recorded for Spatial1 and Phasial. The spatial resolution was measured with the help from a sharp edge in Spatial1. This value of 1.45 μm is fairly close to the theoretical resolution of 1.2 μm. The smallest detectable feature in the reconstructions was a trace of a square of 2 μm (figure 48), which is not very far from the 1.45 μm. This gives some hint that the used definition of "spatial resolution" as the width of the central part of a slope seems somewhat suitable.

When it comes to the phase object Phasial, what seems as a distortion of

the shape of the reconstructed object can be explained. The beam illuminating the object in the holography setup is not round, but elliptical with dimensions of around 30x50 μm which results in a clipping of the square. There was a very low transmittance in the chromium. But more interestingly, the expected phase difference of 1.4 radians between the light traveling through the object and the light traveling besides it, was not obtained.

Further investigations of phase objects are needed. A problem with Phasial might be that it is blocking to much of the light. The results looks similar to applying a high-pass filter. Since no information from the center of the object is present, the general features cannot be reconstructed. This can be seen in the reconstructed phase of the Phasial object (figure 52b), where only the phase shift at the edge is visible. A good idea is to try phase objects of smaller size or higher transmission and study the reconstructed transmission and phase.

Once the phase can be reconstructed successfully, the resolution of phase could most likely also be studied quantitatively by using objects made by microlithography and evaporation. One could then make several layers of smaller and smaller areas forming some kind of step function. One would then look at how small difference in phase of the light, caused by the different thicknesses of the layer, that can be detected. It is then crucial to use a material with low absorption. Another idea is to just see if one can resemble off-line holography by letting the object be a film with two holes in it. This might increase the chance for a clearer image, if the image and twin image then could be separated.

Later exciting tests could be about trying to capture very rapid processes. One could think about exciting plasmons in gold colloids with the infrared pulse and detect a possible change in refractive index effect with the X-UV beam. EBL techniques could be useful here in order to define areas of the colloids as a collective effect might be the most wise to search for. Now that technique has been developed how to perform EBL and evaporation on these thin membranes, the flexibility inherent in the EBL method, gives us a wealth of possibilities.

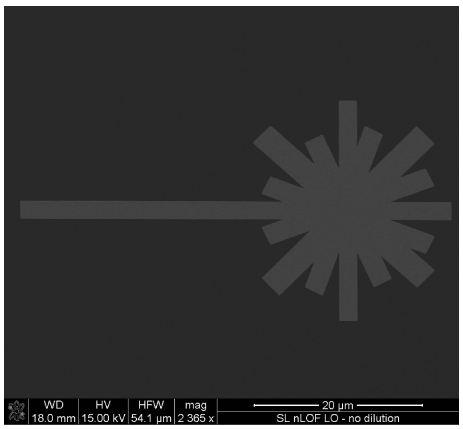

Figure 54: A laser symbol of gold made on a 50 nm silicon nitride window.

Acknowledgements

It has been a privilege to work with this project in many ways. Working with and watching small parts of the world normally unseen is nothing but a privilege in itself. Also, I have been surrounded by people who have strengthened my curiosity and ambition. I am very thankful to Jörg Schwenke who supportingly always had time for helping out. Prof. Anne L'Huillier deserves a warm thank for giving me the possibility to work with this nice project. She also helped by greatly contributing to the very nice atmosphere in the Attosecond group. I am very impressed by the humbleness to science and people that exists in the group. Many warm thanks to all of you: Anders Persson, Christian Erny, Cord Arnold, Erik Mansten, Johan Mauritsson, Kathrin Klünder, Marcus Dahlström, Marko Swoboda, Mathieu Gisselbrecht, Michele Giunta, Miguel Miranda, Per Johnsson, Rafal Rakowski, Thomas Fordell and Xinkui He. Thanks also to the whole division for providing a fantastic platform. Anders Mikkelsen strengthened my playfulness and I really appreciate our talks. This project would not be possible without the great and unlimited support from the staff at the Lund Nano Lab: Ivan Maximov, Anders Kvennerfors, George Rydnemalm and Mariusz Graczyk. The daily challenges I met was handled with comforting guidance by users of the lab, especially by Kristian Storm, Anil Dey and Bahram Ganjipour. Great thanks also to the family and friends around me.

References

[1] R. A. Bartels, A. Paul, H. Green, H. C. Kapteyn, M. M. Murnane, S. Backus, I. P. Christov, Y. Liu, D. Attwood, and C. Jacobsen. Generation of spatially coherent light at extreme ultraviolet wavelengths. *Science*, 297(5580):376–378, 2002.

[2] H. Benson. *University Physics*. John Wiley and Sons, 1996.

[3] R. E. Burge, M. A. Fiddy, A. H. Greenaway, and G. Ross. The phase problem. *Proceedings of the Royal Society of London. Series A, Mathematical and Physical Sciences*, 350(1661):191–212, 1976.

[4] T. H. P. Chang. Proximity effect in electron-beam lithography. *Journal of Vacuum Science and Technology*, 12(6):1271–1275, 1975.

[5] H. N. Chapman, A. Barty, M. J. Bogan, S. Boutet, M. Frank, S. P. Hau-Riege, S. Marchesini, B. W. Woods, S. Bajt, W. H. Benner, R. A. London, E. Plonjes, M. Kuhlmann, R. Treusch, S. Dusterer, T. Tschentscher, J. R. Schneider, E. Spiller, T. Moller, C. Bostedt, M. Hoener, D. A. Shapiro, K. O. Hodgson, D. van der Spoel, F. Burmeister, M. Bergh, C. Caleman, G. Huldt, M. M. Seibert, F. R. N. C. Maia, R. W. Lee, A. Szoke, N. Timneanu, and J. Hajdu. Femtosecond diffractive imaging with a soft-x-ray free-electron laser. *Nature Physics*, 2(12):839–843, 2006.

[6] J. R. Fienup. Phase retrieval algorithms: a comparison. *Applied Optics*, 21(15):2758–2769, 1982.

[7] J. Goldstein, D. Newbury, D. Joy, P. Echlin, C. Lyman, P. Echlin, E. Lifshin, L. Sawyer, and J. Michael. *Scanning electron microscopy and x-ray microanalysis*. Kluwer Academic, 2003.

[8] http://en.wikipedia.org, 20100420.

[9] http://henke.lbl.gov/optical_constants, 20100401.

[10] Michrochem: http://www.microchem.com/products/pdf/PMMA_Data_Sheet.pdf, 20100416.

[11] T. Latychevskaia and H-W. Fink. Solution to the twin image problem in holography. *Phys. Rev. Lett.*, 98(23):233901, 2007.

[12] M. M. Leivo and J. P. Pekola. Thermal characteristics of silicon nitride membranes at sub-kelvin temperatures. *Applied Physics Letters*, 72(11):1305–1307, 1998.

[13] A. Mai. Digital in-line x-uv holography for time resolved microscopy. 2008.

[14] A. Mikkelsen, J. Schwenke, T. Fordell, G. Luo, K. Klünder, E. Hilner, N. Anttu, A. A. Zakharov, E. Lundgren, J. Mauritsson, and J. N. Andersen. Photoemission electron microscopy using extreme ultraviolet attosecond pulse trains. *Review of Scientific Instruments*, 80(12):3095–3097, 2009.

[15] A-S. Morlens, J. Gautier, G. Rey, P. Zeitoun, J-P. Caumes, M. Kos-Rosset, H. Merdji, S. Kazamias, K. Cassou, and M. Fajardo. Generation of spatially coherent light at extreme ultraviolet wavelengths. *Optical Letters*, 31(21):3095–3097, 2006.

[16] A. Ravasio, D. Gauthier, F. R. N. C. Maia, M. Billon, J-P. Caumes, D. Garzella, M. Géléoc, O. Gobert, J-F. Hergott, A-M. Pena, H. Perez, B. Carré, E. Bourhis, J. Gierak, A. Madouri, D. Mailly, B. Schiedt, M. Fajardo, J. Gautier, P. Zeitoun, P. H. Bucksbaum, J. Hajdu, and H. Merdji. Single-shot diffractive imaging with a table-top femtosecond soft x-ray laser-harmonics source. *Phys. Rev. Lett.*, 103(2):028104, 2009.

[17] B. Saleh and M. C. Teich. *Fundamentals of Photonics.* John Wiley and Sons, 2007.

[18] R. L. Sandberg, A. Paul, D. A. Raymondson, S. Hädrich, D. M. Gaudiosi, J. Holtsnider, R. I. Tobey, O. Cohen, M. M. Murnane, H. C. Kapteyn, C. Song, J. Miao, Y. Liu, and F. Salmassi. Lensless diffractive imaging using tabletop coherent high-harmonic soft-x-ray beams. *Phys. Rev. Lett.*, 99(9):098103, Aug 2007.

[19] U. Schnars and W. Jueptner. *Digital Holography.* Springer, 2005.

[20] J. Schwenke, A. Mai, M. Miranda, X. He, G. Genoud, A. Mikkelsen, S-G. Petterson, A. Persson, and A. L'Huillier. Single-shot holography using high-order harmonics. *Journal of Modern Optics*, 55(16):2723–2730, 2008.

[21] R. Y. Stanier, J. L. Ingraham, and M. Wheelis ans P. R. Painter. *General Microbiology.* Prentice Hall, 1986.

[22] S. M. Sze. *Semiconductor devices, physics and technology.* John Wiley and Sons, 2002.